Journal of Metals, Materials and Minerals, 34(4), 2114, 2024

Controlling titanium incorporation in hydrogenated amorphous carbon films via closed-loop feedback in reactive high power impulse magnetron sputtering

Pornthip RATCHAYOTEE[1], Artit CHINGSUNGNOEN[1], and Phitsanu POOLCHARUANSIN[1,*]

[1] *Department of Physics, Faculty of Science, Mahasarakham University, Maha Sarakham 44150, Thailand*

***Corresponding author e-mail**: phitsanu.p@msu.ac.th

Received date:
01 August 2024
Revised date:
25 September 2024
Accepted date:
30 September 2024

Keywords:
Controlling discharge current;
Titanium doped on amorphous carbon;
Reactive high power impulse magnetron sputtering;
Feedback control

Abstract

A closed-loop feedback approach has been developed to control titanium incorporation in hydrogenated amorphous carbon (a-C:H) films during reactive high-power impulse magnetron sputtering (R-HiPIMS). The average discharge current measured at the magnetron target is used as the primary feedback signal to regulate the target coverage state. Hence, the titanium concentration in the films can be controlled. Significant changes were observed in the film microstructure and properties as the target state evolved with increasing target coverage. This causes the film transition from metallic titanium to a-C:H films with decreasing titanium concentration. For example, the XRD and Raman analyses indicated a microstructural change from hexagonal titanium to cubic titanium carbide and finally to amorphous carbon. The change in microstructure aligned with the density decreasing from 4.7 g·cm^{-3} to 1.6 g·cm^{-3} measured by XRR technique. In addition, a decrease in the Ti/C atomic ratio, from 1.53 to 0.03, clearly demonstrates that the titanium content can precisely be controlled. A simplified model was proposed to explain the relationship between the average HiPIMS current and the carbon coverage fraction on the target surface. The suggested relationship clarifies how adjusting the average discharge current effectively regulates the target coverage state and the consequent titanium concentration. The approach not only enhances process stability, but also offers an alternative to traditional control techniques during the deposition process.

1. Introduction

Metal-doped hydrogenated amorphous carbon (a-C:H), a variant of diamond-like carbon (DLC) incorporating metal dopants within C-H network, offers tailored properties to meet diverse and demanding applications. These films consist of a disordered network where carbon atoms exhibit sp^2 (graphitic) and sp^3 (diamond-like) bonding configurations, along with varying concentrations of incorporated metal elements. The introduction of metals, for example, titanium (Ti), tungsten (W), chromium (Cr), silver (Ag), copper (Cu), etc., can enhance properties such as tribology at high temperatures [1], hardness, wear resistance [2], corrosion resistance [3], electrical conductivity [4], and antibacterial characteristics [5]. These functionalities offer significant potential for metal-doped a-C:H films in a wide range of applications, e.g. tribological coatings [6], biomedical devices [7], sensors and emerging electronic technologies [8].

Dopant concentration, whether metal or non-metal species, within a-C:H films can induce structural modification, including shifts in the sp^2/sp^3 bonding ratio, the potential formation of nanoclusters or distinct phases, and significant changes in internal stress, surface properties, and defect density [2,9]. The relationship between dopant concentration and resulting microstructure of a-C:H films is often non-linear. Slight adjustments in concentration can trigger significant shifts in microstructure and properties [10-12]. Precise control over dopant concentration is therefore crucial for achieving the designed characteristics and functionalities in doped a-C:H films.

Reactive magnetron sputtering techniques have been extensively employed for metal-doped a-C:H film deposition. A metal target is used to generate the sputtered dopant species, while hydrocarbon reactive gas (e.g., CH_4, C_2H_2) is employed for C-C and C-H networks in the depositing films. However, during the sputtering process, reactive gas molecules can chemically react with the exposed target surface forming a compound layer. This "target poisoning" phenomenon disrupts the release of metal atoms and leads to fluctuations in dopant incorporation, film properties and reproducibility [13-15].

Close-loop feedback controls have been developed to address the challenges of target poisoning, process stability [16] and precisely tailor dopant concentration in metal-doped a-C:H films during reactive magnetron sputtering [13]. For example, the control process monitors the emission intensity of metal species and dynamically adjusts the flow rate of hydrocarbon gas [13,17,18]. This feedback mechanism ensures consistent dopant incorporation by active compensation for changes in target surface conditions.

This work introduces an approach for controlling titanium incorporation within hydrogenated amorphous carbon films during reactive high-power impulse magnetron sputtering (R-HiPIMS). The approach uses the average discharge current measured at the magnetron target as the primary feedback signal. This parameter effectively regulates

the target coverage state, providing a fast and sensitive response to changes in target surface conditions. A proportional-integral (PI) controller dynamically adjusts the acetylene (C_2H_2) gas flow rate. Thin film characterization demonstrates the effectiveness of this method, which allows precise control over titanium incorporation. Consequently, the film structure and properties can be tailored. This methodology offers an alternative to traditional reactive sputtering control techniques.

2. Experimental setup

2.1 Coating system apparatus

Titanium-doped amorphous carbon (Ti-doped a-C:H) films were prepared using reactive high-power impulse magnetron sputtering (R-HiPIMS) with a closed-loop feedback controller. The setup is shown in Figure 1. A vacuum chamber was evacuated to a base pressure of 10^{-5} Torr. Argon was used as the sputtering gas, and acetylene (C_2H_2) as the reactive gas. A 2-inch diameter titanium target (99.99% purity) was mounted on the magnetron source, powered by an in-house HiPIMS unit (a pulse width of 20 µs, a repetition rate of 400 Hz).

The discharge current and voltage were monitored using probes and displayed on a digital oscilloscope. A proportional-integral (PI) controller adjusted the acetylene flow rate based on the average discharge current, sending a control signal to the mass flow controller. A shutter opened once the current reached a setpoint, ensuring steady-state deposition. Optical emission spectroscopy (OES) was used to analyze plasma emissions from a side-view of the ionization zone. Spectral data (300 nm to 1000 nm, 0.4 nm resolution) were collected with an AvaSpec ULS4096 spectrometer.

2.2. Coating procedure

Polished single-crystal silicon wafers (1 cm × 1 cm) were used as substrates. Before deposition, the wafers were ultrasonically cleaned with acetone, methanol, and deionized water for 15 min each, then dried with nitrogen gas. The substrates were mounted on an electrically grounded holder located 8 cm away from the titanium target.

Argon gas was introduced at 20 sccm, and the chamber pressure was initially set to 8 mTorr. The titanium target was cleaned in argon using a DC power of 100 W for 10 min to 20 min. To identify the setpoints, the average discharge current (I_{avg}) was recorded while the acetylene (C_2H_2) flow rate was gradually increased from 0 sccm to 6.0 sccm. This scanning process was repeated multiple times to ensure the reproducibility of the discharge behavior, which is critical to the deposition process. Once the setpoint was identified, the feedback controller adjusted the acetylene flow to maintain I_{avg} at a specific setpoint.

2.3 Thin film characterization

Several analytical techniques were used to characterize the deposited films. These include a field emission scanning electron microscope (FE-SEM) with the energy-dispersive X-ray spectroscopy (EDS) to analyze morphology and elemental composition. X-ray diffraction (XRD) examined crystalline structure, while X-ray reflectometry (XRR) measured film density and determined the deposition rate. Raman spectroscopy analyzed carbon bonding (sp^2 and sp^3), and X-ray photoelectron spectroscopy (XPS) provided insights into the chemical state and bonding environment of the elements.

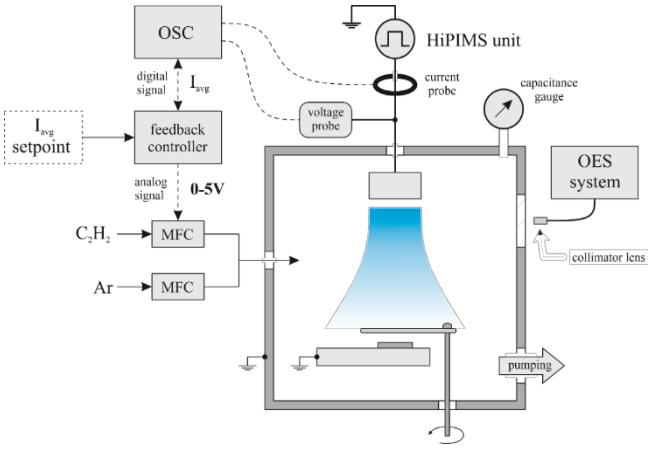

Figure 1. Schematic representation of the experimental arrangement for Ti containing DLC deposition via reactive high power impulse magnetron sputtering technique. A digital oscilloscope (OSC) with voltage and current probes integrated to a feedback controller regulating the mass flow controller (MFC) of C2H−2 gas. An optical emission spectroscopy (OES) system with a collimator lens was employed for plasma diagnostic purposes.

3. Results

In reactive magnetron sputtering, the formation of compound films on the metal target surface triggers the process instability. Specifically, when using acetylene as a reactive gas, the accumulation of carbon layers on the titanium target surface initiates instability in the discharge process, which in turn affects the control over titanium concentrations within the deposited films. This study introduces a feedback approach to control the coverage state of the carbon layer on the titanium surface. The coverage states are categorized into three distinct levels namely uncovered, partially covered, and fully covered. By implementing the feedback control, it is possible to maintain titanium concentration within the a-C:H films. This section is divided into three subsections to demonstrate the effectiveness of the feedback approach in improving the process stability and controlling the structure and composition of the deposited film.

3.1 Discharge characteristics

The discharge current waveforms captured by the oscilloscope during HiPIMS discharges in uncovered and fully covered target states are presented in Figure 2. The uncovered target state is obtained in Ar, while the fully covered state is achieved using the C_2H_2 and Ar at a constant flow rate of 5 sccm and 20 sccm, respectively. A clear difference in the discharge waveforms between these two target states is observed. The peak discharge current in the uncovered target state is close to 40 A, significantly higher than that in the fully covered state (approximately 1 A). This variation in the discharge current waveforms indicates a change in the target surface properties transitioning from an initial titanium surface to one covered by a carbon layer.

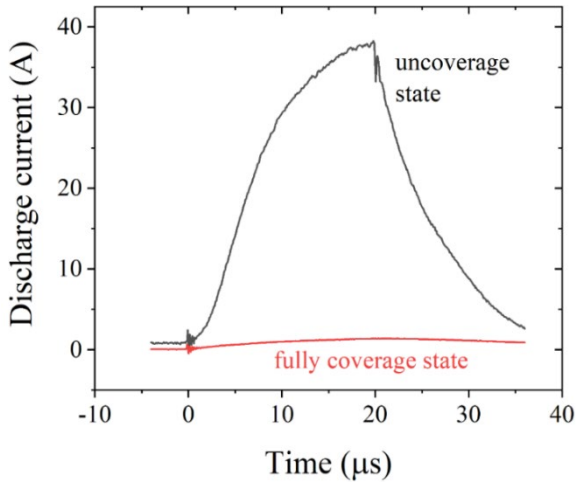

Figure 2. Discharge current waveforms for the target with uncovered state and fully covered state.

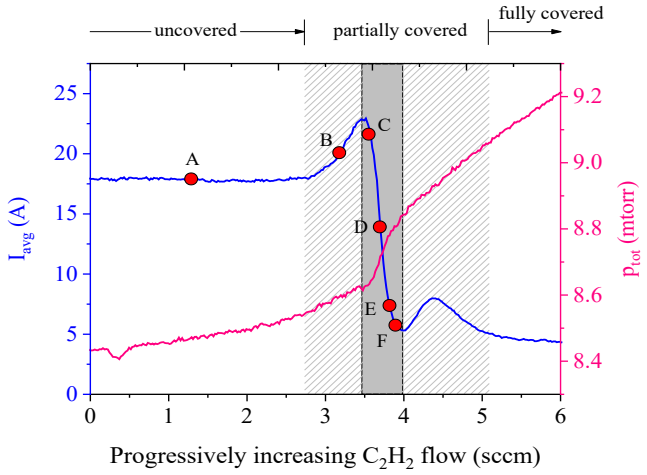

Figure 3. Average discharge current, I_{avg} and total pressure, p_{tot} as functions of progressive acetylene flow during the scanning process. Points A through F on the discharge current curve represent the designed setpoints for feedback control, corresponding to different titanium concentrations in the deposited films.

For the implementation of a feedback algorithm, the use of the discharge current waveform—comprising a 2D array of data—may be ineffective due to the baud rate limitation for data reading from the oscilloscope. Therefore, it is proposed to use the average discharge current, represented by a single numerical data. Consequently, the real-time measurement capability inherent to the oscilloscope is utilized to obtain the average discharge current over the entire acquisition window. It is worth noting that the acquisition window of the oscilloscope needs to be optimized to maintain the sensitivity of the average current.

Figure 3 illustrates the variation of the average discharge current (I_{avg}) and total pressure (p_{tot}) in response to progressively increasing acetylene flow throughout the scanning procedure. The I_{avg} curve defines two stable regions referred to as the uncovered target state at a high current of approximately 18 A and fully covered target state at $I_{avg} \approx 4$ A. Additionally, I_{avg} shows the non-monotonic unstable region associated with the partially covered target state. Notice that within the non-monotonic feature there is the most unstable region where I_{avg} and p_{tot} changes with a fast rate, denoted by the gray area in the graph. The non-monotonic feature is not found in the total pressure curve. This suggests that the I_{avg} curve could capture more detail in the reactive process.

These three regions, as observed in the I_{avg} and p_{tot} curves correspond to the stable metal mode, the stable compound mode, and the unstable transition mode typically found in literature [19]. This characteristic in reactive magnetron sputtering discharges is attributed to the dynamic evolution of target coverage which will later be discussed in more detail.

Points A through F on the I_{avg} curve denote the chosen setpoints for feedback control, corresponding to varied titanium concentrations in the depositing films. These setpoints are selected to assign different target coverage states which are essential for customizing the structure and properties of the films. A designed setpoint, I_{set}, was programmed into the feedback system. The controller continually monitors I_{avg} and dynamically modulates the acetylene flow to align I_{avg} with I_{set} to maintain the deviation below 10%. With the process stabilized through feedback control, plasma emission diagnostics and the coating process for the specified setpoint can then be conducted.

3.2 Plasma emissions

Figure 4 presents the optical plasma emission spectrums normalized at 811.3 nm line (Ar I) for the designed setpoints A to F during the feedback assisted HiPIMS process. Note that the selected standard emission lines of Ar I and Ti I [20] are provided at the bottom to the graph. Each measured spectrum was obtained from the side view of the ionization zone in the HiPIMS discharge, providing a non-invasive method to correlate the average discharge current with the target coverage state.

During the uncovered state at setpoint A, emissions are predominantly from titanium species, particularly in the 300 nm to 500 nm range, which contrasts with the argon emissions in the 700 nm to 950 nm range. This metal-dominated plasma is well-known as the characteristic of a non-reactive HiPIMS discharge, where the dense plasma within the ionization zone effectively excites and ionizes the sputtered metal species [21]. Transitioning to the partially covered state at setpoint B, a noticeable decrease in titanium emissions occurs comparable to those of argon. This reduction is attributed to the carbon-based compound layer beginning to cover the titanium surface, thus reducing the available titanium target surface area for sputtering. As the process advances towards the highly unstable region from setpoints C to F, emissions from titanium species diminish markedly indicating a shift from a metal-dominated to a gas-dominated plasma.

The change in plasma emissions at different setpoints infers the transition in target coverage state from an uncovered titanium surface (setpoint A) to one covered by a carbon-based compound (setpoint F). This transition consequently influences the structure and composition of the deposited films.

3.3 Thin films characterization

This section provides the results in thin film characterization for the different setpoints A to F (as seen Figure 3) which correspond to different target coverage and consequent titanium content in the deposited films.

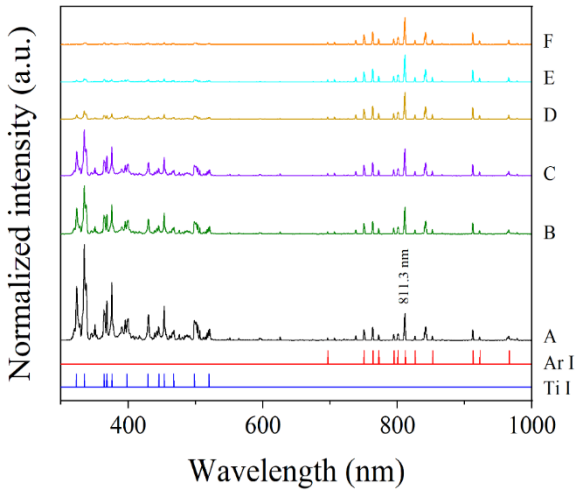

Figure 4. Optical plasma emissions normalized at 811.3 nm (Ar I) for the designed setpoints during the HiPIMS process.

Figure 5(a) shows the density of the deposited films analyzed using XRR technique. There is a clear decreasing trend in the density from setpoint A, with a density of 4.7 g·cm^{-3}, to setpoint F, where the density slightly exceeds 1.6 g·cm^{-3}. The density at setpoint A is close to the density of typical sputtering titanium films [22]. In contrast, the lower density at setpoint F aligns with the typical range for hydrogenated amorphous carbon (a-C:H) films [23].

Grazing incident X-ray diffraction (GIXRD) analysis of the deposited films, as depicted in Figure 5(b), reveals an evolution in crystallographic structures corresponding to various deposition setpoints from A to F. At setpoint A, the XRD pattern correlates with hexagonal titanium, referring to the Powder Diffraction File (PDF) 00-044-1294. The XRD pattern at setpoint B matches with a cubic titanium carbide structure (PDF 03-065-8805). No crystalline peaks are observed from setpoints C to F, except for the silicon peak from the substrate. This indicates that the films deposited between setpoints C and F exhibit a more amorphous which is the typical structure of hydrogenated amorphous carbon (a-C:H) films.

Figure 6 shows the selected SEM images to highlight the most distinct morphological differences. Although the deposition times were adjusted to maintain similar thicknesses for all setpoints, some variation within ± 51 nm was observed in the SEM images. For the film at setpoint A, which is a titanium metal film, one observes a relatively uniform and fine-grained surface structure. The cross-section reveals a dense film with no significate columnar growth or large voids, suggesting a high degree of atomic mobility which is one of the important benefits of the HiPIMS deposition [21,24]. At setpoint B, representing the titanium carbide compound film as examined by XRD analysis, the surface shows a slightly rougher texture compared to position A. The cross-sectional view shows a more defined columnar structure. The film at setpoint F shows a very smooth surface morphology without distinct structures. This kind of morphology is typically found in a-C:H films [25], which agrees with the results from XRR and XRD analyses presented in Figure 5.

EDS analysis, performed on the cross-section SEM images, identified several elements in the deposited films including carbon (C Kα), titanium (Ti L), oxygen (O Kα), aluminum (Al Kα), silicon (Si Kα), and two peaks for titanium (Ti Kα and Ti Kβ). Aluminum, silicon, and oxygen are treated as detected contaminants consistently found in all samples. However, the amount of titanium and carbon significantly changes with the setpoints, represented by the ratio of the atomic percentage between Ti and C, as shown in Figure 7. The Ti/C ratio monotonically decreases from 1.53 to 0.03 from setpoint B to F. This trend suggests a film composition change from titanium-rich to carbon-rich films.

The Raman spectra across different setpoints are shown in Figure 8(a). The spectra with the Raman shift in the range of 1000 cm^{-1} to 1800 cm^{-1} show the typical characteristic of the amorphous carbon with the deconvoluted disorder (D) and graphitic (G) peak [26]. The absence of the carbon characteristic at setpoint A agrees with the previous findings that this setpoint corresponds to crystalline titanium. At setpoint B, the Raman spectrum shows the D and G peaks indicating the formation of the amorphous carbon in the film with the crystalline structure of the TiC as informed by XRD analysis. Presenting the amorphous structure in the film could induce the shortening grain size of the TiC [27] as seen the broadening peaks in the XRD pattern.

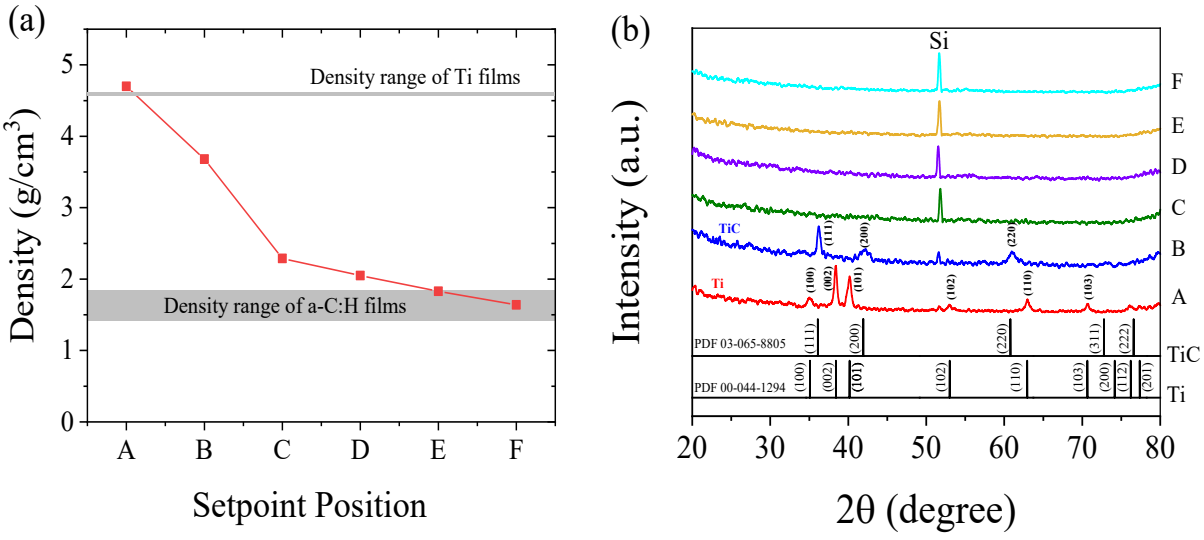

Figure 5. (a) XRR-analysis densities and (b) XRD patterns of the titanium containing hydrogenated amorphous carbon films for the given setpoint positions.

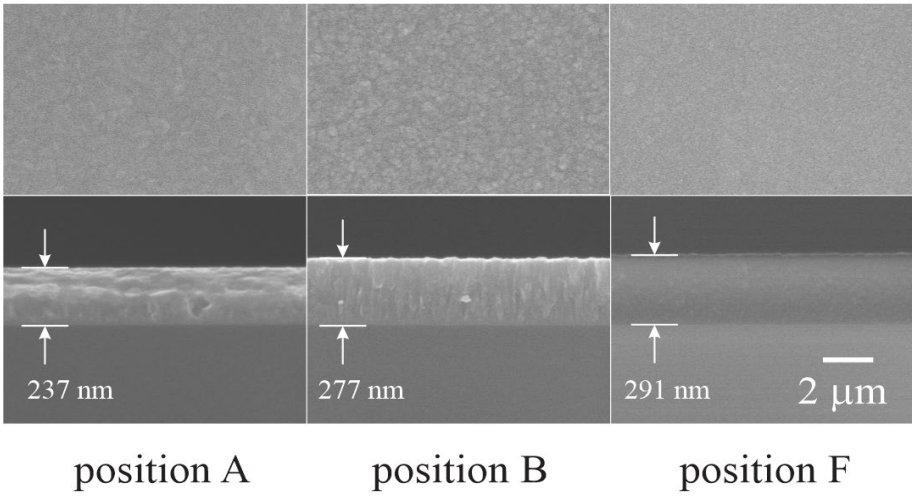

Figure 6. Surface and cross-sectional SEM images at setpoint A, B, and F.

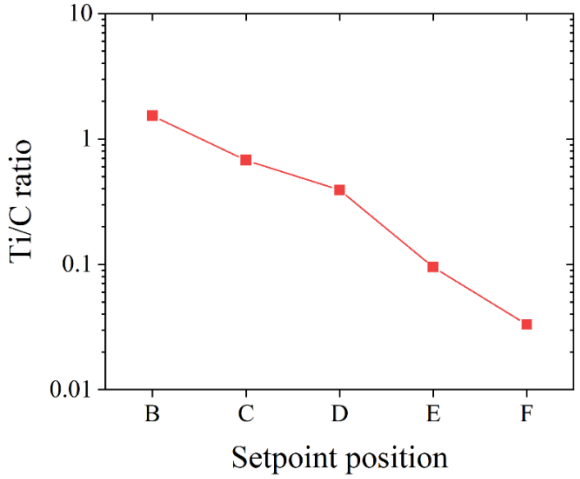

Figure 7. The Ti/C ratio from EDS analysis for different setpoint positions.

The graph in Figure 8(b) is obtained from Raman spectra for amorphous structure across setpoints C to F corresponding toward the low Ti concentration. The integrated area ratio of the D and G peak, I_D/I_G ratio decreases consistently from 4.5 to 1 while the G peak position shifts downward from around 1560 cm^{-1} at setpoint C to 1540 cm^{-1} at setpoint F. The decrease in both I_D/I_G and G peak position informs that the structure of the films transitions from a relatively ordered graphitic network to a more disordered or amorphous state [26] as the titanium concentration decreases (from setpoint C to F). The additional Raman analysis with a broader range (not presented here) confirms the presence of titanium compounds, such as TiC and TiO_2, dominating at setpoint B and becoming negligible toward setpoint F.

The XPS analysis offers a detailed examination of the chemical bonding states within the Ti-doped a-C:H films. A detailed deconvolution of the C1s peak for the sample deposited at setpoint B reveals several bonding states (see Figure 9(a)). The Ti-C peak at around 281.6 eV is attributed to titanium carbide bonds [28]. The C-C peak at around 284.3 eV corresponds to sp^2-hybridized carbon. The C-C peak at approximately 285.0 eV is associated with sp^3-hybridized carbon [29,30]. The peak at around 286.3 eV represents carbon-oxygen single bonds, while the peak near 288.1 eV indicates the presence of carbon-oxygen double bonds [29].

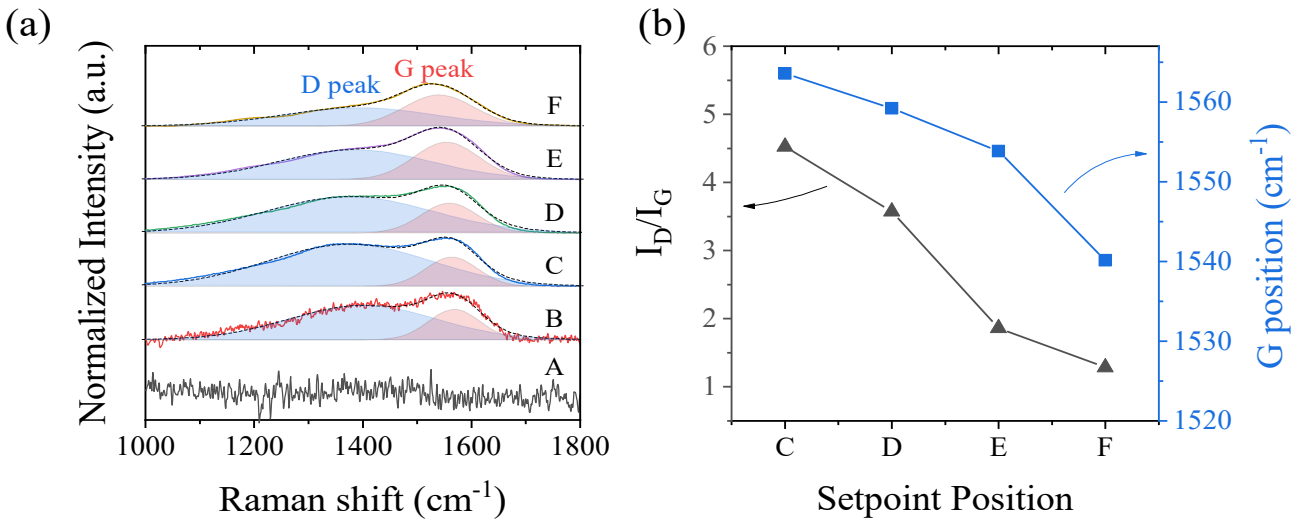

Figure 8. (a) Raman spectra of the deposited films at different setpoints, (b) The area ratio between the deconvoluted D and G peaks and the G peak position.

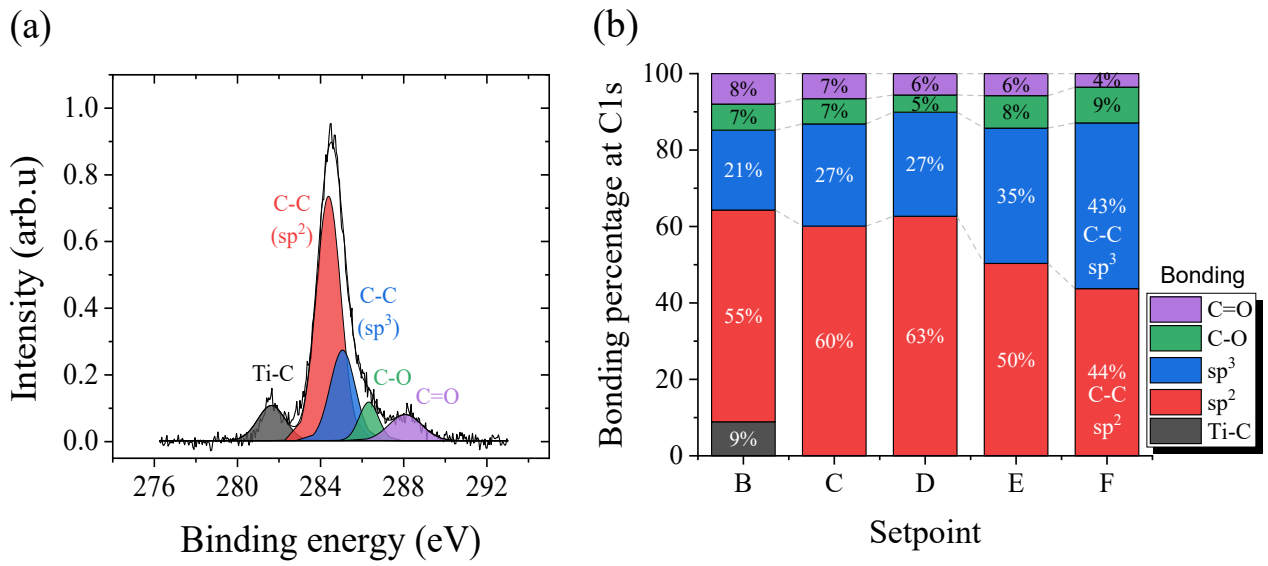

Figure 9. (a) Deconvoluted XPS spectrum of the C1s peak for the sample deposited at setpoint B and (b) bonding percentage distribution at the C1s position for samples deposited at setpoints B to F.

Figure 9(b) illustrated the bonding percentages for samples deposited at setpoints B to F. The Ti-C bonding is present only at setpoint B comprising 9% of the total bonding. The Ti-C peak found in XPS spectrum agrees well with the XRD pattern (see Figure 5(b)), confirming the presence of TiC crystalline structure at this setpoint. The C-C (sp^2) bonding is predominant across all setpoints, though it decreases slightly from 55% at setpoint B to 44% at setpoint F. Conversely, C-C (sp^3) bonding shows an increasing trend, rising from 21% at setpoint B to 43% at setpoint F. This indicates a transition towards a more diamond-like structure as the setpoint charge from B to F. Furthermore, the increase in C-C (sp^3) bonding observed in the XPS analysis correlates with the Raman analysis. As mentioned previously, the decrease in the I_D/I_G ratio and the G peak position in the Raman spectra (Figure 8(b)) indicates a transition from a relatively ordered graphitic network to a more disordered or amorphous state, suggesting a decrease in sp^2 cluster size [26]. The C-O and C=O bonding remains relatively constant (4% to 9%) owing to some degree of surface oxidation or oxygen contamination.

4. Discussion

The experimental results demonstrate that titanium concentration, film composition, microstructure, and chemical bonding state in the deposited films show significant variations with the average HiPIMS current I_{avg}. This correlation is linked to the change in the targe coverage state from uncovered to partially and fully covered states, respectively.

In the uncovered state, the discharge is stable, and the target surface is predominantly titanium resulting in titanium domination in the deposited film. The partially covered state is characterized by unstable discharge due to the competition between the formation and sputtering of carbon-based compound layers on the target surface [19]. Once the compound layer completely covers the target surface, the target is in the fully covered state, leading to the titanium-less feature in the deposited film.

The behavior described above is a well-known characteristic in reactive magnetron sputtering processes. The deposition by a constant flow of the reactive gas is unsuitable to regulate the target state and consequent titanium concentration, especially during the partially covered state. The average HiPIMS current I_{avg}, however, effectively regulates the target state. This regulation is related to the fraction ($\phi_C = A_C/A_{tar}$) of the accumulated carbon area A_C on the target surface A_{tar}. We could simplify the relation between I_{avg} and ϕ_C by the following relationships.

$$I_{avg} = K + m\phi_C \quad (1)$$

where K and m relates to secondary electron emission yield of the titanium $\gamma_{se,Ti}$ and carbon $\gamma_{se,C}$ surface, the particle flux of singly charged ions bombarding at the target surface Γ_{ion} and fundamental charge e, expressed as

$$K = (1+\gamma_{se,Ti})(eA_{tar}\Gamma_{ion}) \quad (2)$$

$$m = (\gamma_{se,C} - \gamma_{se,Ti})(eA_{tar}\Gamma_{ion}) \quad (3)$$

At setpoint A, the target state is initially uncovered, i.e., $\phi_C = 0$. The recorded I_{avg} and the depositing films at setpoint A result from the clean titanium surface. When introducing the C_2H_2 at setpoints B to F, the carbon compound layer is progressively formed on the titanium target. The target state changes to the partially covered state. The average discharge current I_{avg} tends to decrease due to the lower secondary electron emission yield of the carbon compound layer $\gamma_{se,C}$ [31], compared to $\gamma_{se,Ti}$ [32]. Consequently, the concentration of titanium in the deposition films gradually reduces due to the diminishing exposed titanium area on the target surface.

At setpoint B, the exposed titanium area is still large. The amount of titanium and carbon in the deposition films can be comparable, forming the crystal structure of titanium carbide films on the substrate

surface. At setpoints C to F, however, the carbon-covered area continuously expands, indicated by the reduction of I_{avg}. This causes a decrease in the titanium exposed area and sputtered titanium flux. Consequently, amorphous carbon films with reduced titanium concentration are formed during these setpoints.

This study highlights that through precise control of I_{avg}, the target coverage state can be effectively adjusted with the assistance of feedback control. Therefore, the composition and properties of the carbon films can be tailored. The findings provide an alternative approach for achieving controlled titanium incorporation in hydrogenated amorphous carbon films via closed-loop feedback during reactive HiPIMS. This approach not only enhances process stability but also allows precise tuning of the metal dopant concentration in amorphous carbon films. This enables fine adjustments in microstructure, chemical bonding, and consequent film properties.

5. Conclusions

Titanium-doped diamond-like carbon (DLC) films were prepared using the reactive high-power impulse magnetron sputtering technique assisted by a closed-loop feedback approach. The results show that the average HiPIMS current, used as the feedback parameter, effectively regulates the target coverage state. This regulation technique significantly impacts plasma emission, composition, microstructure, and chemical bonding state in the deposited films. Particularly, during the unstable partially covered state, the titanium-to-carbon ratio can be controlled within a range of 0.70 to 0.03, allowing adjustments in film density, I_D/I_G ratio, and C-C bonding. The simplified model suggests a linear relationship between the average HiPIMS current and the carbon area fraction on the target surface. Therefore, controlling the feedback of the average discharge current enhances the stability of the reactive HiPIMS process and allows precise tailoring of the structure and properties of the films.

Acknowledgment

This research was financially supported by the Faculty of Science, Mahasarakham University. The authors gratefully acknowledge all facilities and technical support from the Synchrotron Light Research Institute (Public Organization).

References

[1] Q. Zeng, and Z. Ning, "High-temperature tribological properties of diamond-like carbon films: A review," *Reviews on Advanced Materials Science*, vol. 60, no. 1, pp. 276-292, 2021.

[2] O. Sharifahmadian, A. Pakseresht, K. K. Amirtharaj Mosas, and D. Galusek, "Doping effects on the tribological performance of diamond-like carbon coatings: A review," *Journal of Materials Research and Technology*, vol. 27, pp. 7748-7765, 2023.

[3] B. Mi, Q. Wang, Y. Xu, Z. Qin, Z. Chen, and H. Wang, "Improvement in corrosion resistance and interfacial contact resistance properties of 316L stainless steel by coating with Cr, Ti Co-doped amorphous carbon films in the environment of the PEMFCs," *Molecules*, vol. 28, no. 6, p. 2821, 2023.

[4] M. Grischke, K. Bewilogua, K. Trojan, and H. Dimigen, "Application-oriented modifications of deposition processes for diamond-like-carbon-based coatings," *Surface and Coatings Technology*, vol. 74–75, pp. 739–745, 1995.

[5] I. Carvalho, L. Rodrigues, M. J. Lima, S. Carvalho, and S. M. A. Cruz, "Overview on the antimicrobial activity and biocompatibility of sputtered carbon-based coatings," *Processes*, vol. 9, no. 8, p. 1428, 2021.

[6] I. Bouabibsa, S. Lamri, and F. Sanchette, "Structure, mechanical and tribological properties of Me-doped diamond-like carbon (DLC) (Me = Al, Ti, or Nb) hydrogenated amorphous carbon coatings," *Coatings,* vol. 8, no. 10, p. 370, 2018.

[7] A. Schroeder, G. Francz, A. Bruinink, R. Hauert, J. Mayer, and E. Wintermantel, "Titanium containing amorphous hydrogenated carbon films (a-C : H/Ti): surface analysis and evaluation of cellular reactions using bone marrow cell cultures in vitro," *Biomaterials,* vol. 21, no. 5, pp. 449-456, 2000.

[8] D. Virganavičius, V. J. Cadarso, R. Kirchner, L. Stankevicius, T. Tamulevicius, S. Tamulevicius, and H. Schift, "Patterning of diamond like carbon films for sensor applications using silicon containing thermoplastic resist (SiPol) as a hard mask," *Applied Surface Science*, vol. 385, pp. 145-152, 2016.

[9] X. Pang, L. Shi, P. Wang, Y. Xia, and W. Liu, "Effects of Al incorporation on the mechanical and tribological properties of Ti-doped a-C:H films deposited by magnetron sputtering," *Current Applied Physics*, vol. 11, no. 3, pp. 771-775, 2011.

[10] P. Safaie, A. Eshaghi, and S. R. Bakhshi, "Structure and mechanical properties of oxygen doped diamond-like carbon thin films," *Diamond and Related Materials*, vol. 70, pp. 91-97, 2016.

[11] L. Chen, J. Wu, Z. Lu, L. Shang, G. Zhang, and Q. Xue, "Probing tribological performances of hydrogenated amorphous carbon film applied in methane by structural modification with boron," *Wear,* vol. 470-471, p. 203610, 2021.

[12] R. Z. Moghadam, M. H. Ehsani, H. R. Dizaji, P. Kameli, and M. Jannesari, "Oxygen doping effect on wettability of diamond-like carbon films," *Materials Research Express*, vol. 8, no. 3, p. 035601, 2021.

[13] C.-L. Chang and F.-C. Yang, "Synthesis and characteristics of nc-WC/a-C:H thin films deposited via a reactive HIPIMS process using optical emission spectrometry feedback control," *Surface and Coatings Technology*, vol. 350, pp. 1120-1127, 2018.

[14] M.-Y. Tsai, M-S. Huang, L-K. Chen, Y-D. Shem, M-H. Lin, Y-C. Chiang, K-L. Ou, S-F. Ou, "Surface properties of copper-incorporated diamond-like carbon films deposited by hybrid magnetron sputtering," *Ceramics International*, vol. 39, no. 7, pp. 8335-8340, 2013.

[15] S.-Y. Chen, K.-L. Ou, W.-C. Huang, K.-T. Chu, and S.-F. Ou, "Phase transformation of diamond-like carbon/silver composite films by sputtering deposition," *Ceramics International*, vol. 39, no. 3, pp. 2575-2580, 2013.

[16] T. Shimizu, M. Villamayor, D. Lundin, and U. Helmersson, "Process stabilization by peak current regulation in reactive high-power impulse magnetron sputtering of hafnium nitride," *Journal of Physics D: Applied Physics*, vol. 49, no. 6, p. 065202, 2016.

[17] X. Jiang, F.-C. Yang, J.-W. Lee, and C.-L. Chang, "Effect of an optical emission spectrometer feedback-controlled method on the characterizations of nc-TiC/a-C:H coated by high power impulse magnetron sputtering," *Diamond and Related Materials*, vol. 73, pp. 19-24, 2017.

[18] G. Li, Y. Xu, and Y. Xia, "Effect of Cr atom plasma emission intensity on the characteristics of Cr-DLC films deposited by pulsed-DC magnetron sputtering," *Coatings*, vol. 10, no. 7, p. 608, 2020.

[19] K. Strijckmans, R. Schelfhout, and D. Depla, "Tutorial: Hysteresis during the reactive magnetron sputtering process," J*ournal of Applied Physics*, vol. 124, no. 24, p. 241101, 2018.

[20] "NIST: Atomic Spectra Database Lines Form." Accessed: Jul. 19, 2024. [Online]. Available: https://physics.nist.gov/PhysRefData/ASD/lines_form.html

[21] K. Sarakinos, J. Alami, and S. Konstantinidis, "High power pulsed magnetron sputtering: A review on scientific and engineering state of the art," *Surface and Coatings Technology*, vol. 204, no. 11, pp. 1661-1684, 2010.

[22] K. Drogowska, Z. Tarnawski, A. Brudnik, E. Kusior, M. Sokotowski, K. Zakrzewska, A. Reszka, N.-T.H. Kim-Ngan, and A. G. Balogh, "RBS, XRR and optical reflectivity measurements of Ti–TiO_2 thin films deposited by magnetron sputtering," *Materials Research Bulletin*, vol. 47, no. 2, pp. 296-301, 2012.

[23] N. G. Chechenin, P. N. Chernykh, V. S. Kulikauskas, Y. T. Pei, D. Vainshtein, and J. T. M. D. Hosson, "On the composition analysis of nc-TiC/a-C:H nanocomposite coatings," *Journal of Physics D: Applied Physics*, vol. 41, no. 8, p. 085402, 2008.

[24] M. Samuelsson, D. Lundin, J. Jensen, M. A. Raadu, J. T. Gudmundsson, and U. Helmersson, "On the film density using high power impulse magnetron sputtering," *Surface and Coatings Technology*, vol. 205, no. 2, pp. 591-596, 2010.

[25] D. K. Rajak, A. Kumar, A. Behera, and P. L. Menezes, "Diamond-like carbon (DLC) coatings: Classification, properties, and applications," *Applied Sciences*, vol. 11, no. 10, p. 4445, 2021.

[26] J. Robertson, "Diamond-like amorphous carbon," *Materials Science and Engineering: R: Reports*, vol. 37, no. 4-6, pp. 129-281, 2002.

[27] E. Lewin, O. Wilhelmsson, and U. Jansson, "Nanocomposite nc-TiC/a-C thin films for electrical contact applications," *Journal of Applied Physics,* vol. 100, no. 5, p. 054303, 2006.

[28] M. Zhang, T. Xie, X. Qian, Y. Zhu, and X. Liu, "Mechanical properties and biocompatibility of Ti-doped diamond-like carbon films," *ACS Omega*, vol. 5, no. 36, pp. 22772-22777, 2020.

[29] K. A. M. Aboua, N. Umehara, H. Kousaka, T. Tokoroyama, M. Murashima, M. M. Mustafa, Y. Mabuchi, T. Higuchi, and M. Kawaguchi, "Effect of mating material and graphitization on wear of a-C:H coating in boundary base oil lubrication," Tribology Letters, vol. 68, no. 1, p. 24, 2020.

[30] M. Haneef, M. Evaristo, A. Morina, L. Yang, and B. Trindade, "New nanoscale multilayer magnetron sputtered Ti-DLC/DLC coatings with improved mechanical properties," *Surface and Coatings Technology*, vol. 480, p. 130595, 2024.

[31] L. Liu, F. Lu, J. Tian, S. Xia, and Y. Diao, "Electronic and optical properties of amorphous carbon with different sp3/sp2 hybridization ratio," *Applied Physics A*, vol. 125, no. 5, p. 366, 2019.

[32] D. Depla, G. Buyle, J. Haemers, and R. De Gryse, "Discharge voltage measurements durig magnetron sputtering," *Surface and Coatings Technology*, vol. 200, no. 14-15, pp. 4329-4338, 2006.